International Journal of Advanced Chemistry, 6 (1) (2018) 26-36

International Journal of Advanced Chemistry

Website: www.sciencepubco.com/index.php/IJAC
doi: 10.14419/ijac.v6i1.8719
Research paper

Nonlinear optical investigation of (E)-1-(4-flourobenzylidene)urea using theoretical calculations

J. Tracy [1], A. Dhandapani [2], S. Bharanidharan [3] *

[1] *Department of Physics, PRIST University, Chennai Campus, Mahabalipuram-603 102, India*
[2] *Department of Chemistry, CK College of Engineering and Technology,Cuddalore-607 003, India*
[3] *Department of Physics, Bharath Institute of Higher Education and Research, Bharath University,Chennai-600 073, India*
**Corresponding author E-mail: bharani.dharan0@gmail.com*

Abstract

The FT-IR and FT-Raman spectra of (E)-1-(4-flourobenzylidene)urea (4FBU) was recorded and analyzed. The optimized geometrical parameters were calculated. The complete vibrationally assignments were performed based on PED analysis with the help of SQM method. NBO analysis was carried out to explore the various conjucative/hyperconjucative interactions within the molecule and their second-order stabilization energy. The HOMO and LUMO energy gap was studied. All theoretical calculations were performed based on B3LYP/6-31G (d,p) level of theory. The first order hyperpolarizability (β_0) and related properties (β, α_0, Δ_α) of 4FBU were calculated. Besides, FMOs, MEP, Mulliken atomic charges and various thermodynamic parameters such as entropy, heat capacity and enthalpy were also calculated.

Keywords: *DFT; FT-IR; FT-Raman; NLO; NBO; FMO.*

1. Introduction

The >C=NH-group is present in Schiff base organic molecules are of fundamental importance. They have got extensive application in biological and industrial fields. Schiff bases with a potential pharmaceutical use were synthesized (Charles, 1955; Compagnic Franosise Dereaffinage, 1956). Schiff bases have been reported for their biologic properties, such as anti-bacterial, anti-fungal, anti-inflammatory, analgesic, anti-convulsant, anti-tubercular, anti-cancer, anti-oxidant and anti-helmintic activities (Mounika et al. 2010; Venkatesh, 2011; Yıldız et al. 2004; Ünver et al. 2005; Yıldız et al. 2005; Yıldız, and Dülger, 2005; Yildiz et al. 2007; Kiraz et al. 2009; Sondhi, et al. 2006). Schiff base metal complexes have applications in the areas from material science to biological sciences. They have been widely studied because they have anticancer and herbicidal applications (Cozzi, 2004; Chandra and Sangeetika, 2004).
Numerous studies on Schiff base hydrazones of pyridoxal phosphate, and its analogous have been reported to understanding the mechanism of action for vitamin B6 containing free ligand. Furthermore, metal complexes of hydrazones proved to have potential applications as catalysts (Whitnall et al., 2006), luminescent probes (Spek, 1998), and molecular sensors (Pérez-Rebolledo et al., 2006). Moreover, it has been recently observed that hydrazone's iron chelators in vivo and in vitro, and may be of potential value for the treatment of iron overload (Buss et al. 2002). Kaya & Kamaci, 2012, synthesized novel low band gap and thermally stable poly (azomethine-urethane)s to investigate aliphatic and aromatic group effects on some physical properties such as thermal stability, optical and electrochemical properties.
Dincalpa et al. 2010 synthesized a series of new azo dyes containing salicylal dimine with different electron-withdrawing groups. They studied the absorption and emission spectra of the synthesized salicylal dimine-based azo ligands in five solvents of different polarities. The optical and electrochemical properties were studied, and photovoltaic performance of DSSCs based on these new type salicylal dimine compounds was also investigated.
In our study, focus of the above factors, we have chosen a simple organic molecule (E)-1-(4-fluorobenzylidene) urea for the present investigation. The synthesized molecule is confirmed structurally by the spectral studies. Further the molecule is subjected to the theoretical investigation to study the nonlinear property of the synthesized molecule. In addition to that, the light harvesting efficiency has been calculated to find out its sensitizing property on the application to DSSC. Moreover, the intra-molecular studies are made over to interpret the properties of the molecule.

2. Experimental details

2.1. Synthesis of (E)-1-(4-flourobenzylidene) urea

Equimolar amount of 4-fluorobenzaldehyde and urea were dissolved in 30 ml of absolute ethanol. The mixture was shaken to make homogenous solution. Few drops of catalyst acetic acid were added to increase the rate of reaction. The content was refluxed at 90°C for 3 hours. The completion of the reaction was monitored by thin layer chromatography. After the reaction was completed, the content was cooled the mixture was poured into water. The solid product obtained was filtered and purified using absolute ethanol.

Melting point = 174˚C
Yield = 78%

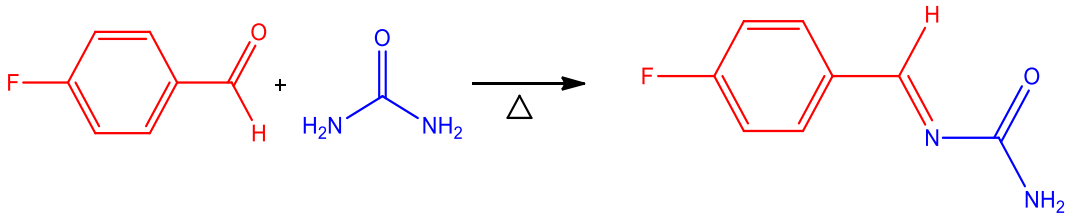

(*E*)-1-(4-fluorobenzylidene)urea

2.2. Spectral measurements

2.2.1. FT-IR spectrum

The FT-IR spectrum of the synthesized 4FBU was measured in the 4000–400 cm^{-1} region at the spectral resolution of 4 cm^{-1} using on SHIMADZU FT-IR affinity Spectrophotometer (KBr pellet technique) in Faculty of Marine Biology, Annamalai University, Parangipettai.

2.2.2. FT-Raman spectrum

The FT-Raman spectrum was recorded on BRUKER: RFS27 spectrometer operating at laser 100mW in the spectral range of 4000–50 cm^{-1}. FT-Raman spectral measurements were carried out from Sophisticated Analytical Instrument Facility (SAIF), Indian Institute of Technology (IIT), Chennai.

2.2.3. NMR spectra

NMR spectral studies were carried out using Bruker 400 MHz spectrometer, using TMS as an internal standard and DMSO-d6 as solvent and recorded at Annamalai University, Annamalainagar, Chidambaram. The ^{1}H and ^{13}C-NMR spectrum were shown in Fig. 9.

3. Computational details

To prove complete information regarding to the structural characteristics and the fundamental vibrational modes of 4FBU has been carried out using DFT method with B3LYP/6-31G (d,p) basis set. The calculations were performed using the Gaussian 03W program package (Frisch et al. 2004; Schlegel, 1982) with default convergence criteria without any constraint on the geometry. The Vibrational modes were assigned on the basis of TED analysis using VEDA4 program package (Jamróz et al. 2006). The Raman activity was calculated by using Gaussian 03W package and the activity was transformed into Raman intensity using Raint program (Michalska, 2003) by the expression:

$$I_i = 10^{-12} \times (\nu_0 - \nu_i)^4 \times \frac{1}{\nu_i} \times RA_i \quad (1)$$

Where I_i is the Raman intensity, RA_i is the Raman scattering activities, ν_i is the wavenumber of the normal modes and ν_0 denotes the wavenumber of the excitation laser (Michalska & Wysokiński, 2005).

4. Results and discussion

4.1. Molecular geometry

The molecular structure along with the numbering of atoms of (E)-1-(4-flourobenzylidene)urea is obtained from Gaussian programs and is shown in Fig. 1. The bond parameters such as bond lengths, bond angles and dihedral angles values are calculated at DFT/B3LYP/6-31G(d,p) level of basis set and are listed in Table 1.

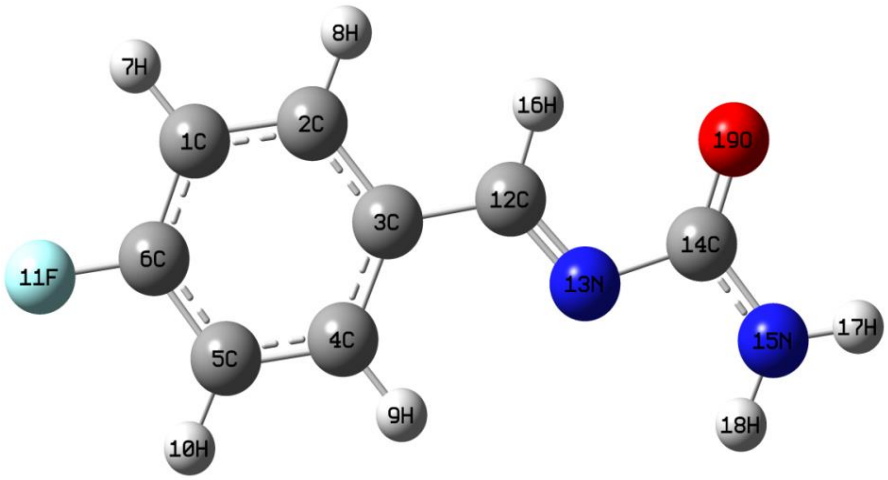

Fig. 1: The Optimized Molecular Structure of 4FBU.

Table 1: The Bond Parameters of 4FBU

Bond Lengths (Å)	DFT	Bond Angles (°)	DFT	Dihedral Angles (°)	DFT
R(1,2)	1.3922	A(2,1,6)	118.3148	D(6,1,2,3)	0.0001
R(1,6)	1.3905	A(2,1,7)	122.0041	D(6,1,2,8)	180
R(1,7)	1.0841	A(6,1,7)	119.6811	D(7,1,2,3)	180.0001
R(2,3)	1.4045	A(1,2,3)	120.9037	D(7,1,2,8)	0
R(2,8)	1.0865	A(1,2,8)	119.6746	D(2,1,6,5)	0
R(3,4)	1.4074	A(3,2,8)	119.4217	D(2,1,6,11)	180.0001
R(3,12)	1.4618	A(2,3,4)	119.1403	D(7,1,6,5)	-180
R(4,5)	1.388	A(2,3,12)	119.2886	D(7,1,6,11)	0.0001
R(4,9)	1.0844	A(4,3,12)	121.5712	D(1,2,3,4)	-0.0001
R(5,6)	1.3947	A(3,4,5)	120.6185	D(1,2,3,12)	180.0001
R(5,10)	1.0844	A(3,4,9)	118.4749	D(8,2,3,4)	-180.0001
R(6,11)	1.3458	A(5,4,9)	120.9066	D(8,2,3,12)	0.0001
R(12,13)	1.2839	A(4,5,6)	118.6305	D(2,3,4,5)	0.0001
R(12,16)	1.0973	A(4,5,10)	121.9439	D(2,3,4,9)	-179.9995
R(13,14)	1.4381	A(6,5,10)	119.4255	D(12,3,4,5)	-180.0001
R(14,15)	1.359	A(1,6,5)	122.3922	D(12,3,4,9)	0.0003
R(14,19)	1.2226	A(1,6,11)	118.8863	D(2,3,12,13)	-180.0021
R(15,17)	1.0065	A(5,6,11)	118.7215	D(2,3,12,16)	-0.0056
R(15,18)	1.0062	A(3,12,13)	122.7784	D(4,3,12,13)	-0.0019
		A(3,12,16)	117.1783	D(4,3,12,16)	179.9945
		A(13,12,16)	120.0432	D(3,4,5,6)	-0.0001
		A(12,13,14)	114.3216	D(3,4,5,10)	179.9999
		A(13,14,15)	110.0043	D(9,4,5,6)	-180.0005
		A(13,14,19)	126.0266	D(9,4,5,10)	-0.0005
		A(15,14,19)	123.9691	D(4,5,6,1)	0.0001
		A(14,15,17)	119.192	D(4,5,6,11)	-180.0001
		A(14,15,18)	119.9422	D(10,5,6,1)	180
		A(17,15,18)	120.8657	D(10,5,6,11)	-0.0001
				D(3,12,13,14)	179.9956
				D(16,12,13,14)	-0.0008
				D(12,13,14,15)	179.9779
				D(12,13,14,19)	-0.0198
				D(13,14,15,17)	179.9952
				D(13,14,15,18)	0.0276
				D(19,14,15,17)	-0.0071
				D(19,14,15,18)	-179.9747

4.2. Non-linear optics

The first hyperpolarizabilities (β_0, α_0 and $\Delta\alpha$) of 4FBU molecule is calculated using B3LYP/6-31G (d,p) basis set, based on the finite-field approach. In the presence of an applied electric field, the energy of a system is a function of the electric field. First hyperpolarizability is a third rank tensor that can be described by a 3x3x3 matrix. The 27 components of the 3D matrix can be reduced to 10 components by Kleinman symmetry (Kleinman, 1962). It can be given in the lower tetrahedral format. It is obvious that the lower part of the 3x3x 3 matrixes is a tetrahedral. The components of β are defined as the coefficients in the Taylor series expansion of the energy in the external electric field. When the external electric field is weak and homogeneous, this expansion becomes:

$$E = E^0 - \mu_\alpha F_\alpha - 1/2\alpha_{\alpha\beta} F_\alpha F_\beta - 1/6\beta_{\alpha\beta\gamma} F_\alpha F_\beta F_\gamma \quad (2)$$

Where E^0 is the energy of the unperturbed molecules, F_α is the field at the origin, and $\mu_\alpha, \alpha_{\alpha\beta}, \beta_{\alpha\beta\gamma}$ are the components of the dipole moment, polarizability and the first hyperpolarizabilities, respectively. The total static dipole moment μ, the mean polarizability α_0, the anisotropy of polarizability Δα and the mean first hyperpolarizability β_0, using the x, y, z components (Alyaret al. 2007) are defined as

$$\mu = (\mu_x^2 + \mu_y^2 + \mu_z^2)^{1/2} \quad (3)$$

$$\alpha_0 = \frac{\alpha_{xx} + \alpha_{yy} + \alpha_{zz}}{3} \quad (4)$$

$$\Delta\alpha = 2^{-1/2}\left[\begin{array}{l}(\alpha_{xx} - \alpha_{yy})^2 + (\alpha_{yy} - \alpha_{zz})^2 + \\ (\alpha_{zz} - \alpha_{xx})^2 + 6(\alpha_{xy}^2 + \alpha_{yz}^2 + \alpha_{xz}^2)\end{array}\right]^{1/2} \quad (5)$$

$$\beta_0 = (\beta_x^2 + \beta_y^2 + \beta_z^2)^{1/2} \quad (6)$$

Many organic molecules, containing conjugated π electrons are characterized by large values of first hyperpolarizabilities, were analyzed by means of vibrational spectroscopy (Castiglioni et al. 1995; Zuliani et al. 1995; Del Zoppo et al., 1995; Del Zoppo et al. 1998). The intra-molecular charge transfer from the donor to acceptor group through a single-double bondconjugated path can induce large variations of both the molecular dipole moment and the molecular polarizability, making IR and Raman activity strong at the same time (Ravikumar et al. 2008).

Theoretical investigation plays an important role in understanding the structure property relationship, which is able to assist in designing novel NLO materials. It is well known that the higher values of dipole moment, molecular polarizability and hyperpolarizability are important for more active NLO properties. The present study reveals that the π-π interaction can make larger intra-molecular interaction and hence the polarizability of the molecule increases. It is evident to Table (2), the molecular dipole moment (μ), molecular polarizability and hyperpolarizability are calculated about 2.0705 (D), 5.7250 and 10.5890×10^{-30}esu, respectively. The β_0 value of the title compound is twenty eight times greater than that of reference urea. Hence, our title molecule is an interesting object for Non-linear Optics.

Table 2: The Non-Linear Optical Properties of 4FBU

Parameters	B3LYP/6-31G(d,p)
Dipole moment (μ)	Debye
μ_x	-0.5194
μ_y	-2.0017
μ_z	0.1030
M	2.0705Debye
Polarizability (α_0)	$x10^{-30}$esu
α_{xx}	241.55
α_{xy}	-23.64
α_{yy}	281.26
α_{xz}	-7.02
α_{yz}	17.27
α_{zz}	149.10
A	$5.7250x10^{-30}$esu
Hyperpolarizability (β_0)	$x10^{-30}$esu
β_{xxx}	542.29
β_{xxy}	271.19
β_{xyy}	457.42
β_{yyy}	-1008.01
β_{xxz}	-105.22
β_{xyz}	56.53
β_{yyz}	-11.69
β_{xzz}	-6.03
β_{yzz}	38.61
β_{zzz}	-48.65
β_0	$10.5890x10^{-30}$esu

Reference value of urea (μ=1.3732 Debye, β_0=$0.3728x10^{-30}$esu): esu-electrostatic unit

4.3. NBO analysis

NBO analysis provides an efficient method for studying intra and inter-molecular bonding and interaction among bonds, and provides a convenient basis for investigation charge transfer or conjugative interactions in the molecular system. Another useful aspect of NBO method is that it gives information about interactions in both filled and virtual orbital spaces that could enhance the analysis of intra and inter-molecular interactions. The hyper conjugation may be given as stabilizing effect that arises from an overlap between an occupied orbital with another neighboring electron deficient orbital when these orbitals are properly orientation. This non-covalent bonding and anti-bonding interaction can be quantitatively described in terms of the NBO analysis, which is expressed by means of the second-order perturbation interaction energy ($E^{(2)}$) (Reed&Weinhold, 1985; Reed et al. 1985; Reed&Weinhold, 1983; Foster&Weinhold, 1980). this energy represents the estimation of the off-diagonal NBO Fock matrix elements. It can be deduced from the second-order perturbation approach (Chocholoušová et al. 2004).

$$E^{(2)} = \Delta E_{ij} = q_i \frac{F(i,j)^2}{\varepsilon_j - \varepsilon_i} \quad (7)$$

Where, qi is the donor orbital occupancy, εi and εj are diagonal elements (orbital energies) and F (i, j) is off diagonal NBO Fock matrix elements.

NBO analysis was performed by the B3LYP level of theory with 6-31G (d,p) basis set for the molecule 4FBU. NBO theory allows the assignment of hybridization of atomic lone pairs and of the atoms involved in bond orbitals. These are important data in spectral interpretation as the frequency ordering is related to the bond hybrid composition. The second order perturbation energy values $E^{(2)}$ collected in Table 3 reveals the important interactions between the Lewis and non-Lewis type NBO orbitals of 4FBU molecular system. In the present case, the intra-molecular hyperconjucative interactions are formed by the orbital overlap between bonding (C-C), (C-N) and anti-bonding (C-C), (C-O), (C-N) orbitals. The lone pair electrons from N, O and F atoms have also shown interactions with anti-bonding orbitals of (C-C, (C-O) and (C-N), which results in the stabilization of 4FBU molecular system.

Table 3: The Second Order Fock Matrix of 4FBU

Type	Donor (i)	ED (e)	Acceptor (j)	ED (e)	$E^{(2)}$ KJ/mol	$E^{(2)}$ Kcal/mol	E(j)-E(i) a.u.	F(i,j) a.u.
π -π*	C1-C6	1.6439	C2-C3	0.3792	92.97	22.22	0.3	0.073
			C4-C5	0.2888	68.07	16.27	0.3	0.063
π -π*	C2-C3	1.6273	C1-C6	0.3671	77.61	18.55	0.27	0.063
			C4-C5	0.2888	87.82	20.99	0.28	0.07
			C12-N13	0.1278	83.47	19.95	0.28	0.071
π -π*	C4-C5	1.6844	C1-C6	0.3671	100.92	24.12	0.27	0.074
			C2-C3	0.3792	70.63	16.88	0.28	0.063
π -π*	C12-N13	1.8904	C2-C3	0.3792	33.56	8.02	0.34	0.05
			C14-O19	0.3321	87.86	21	0.34	0.08
n -σ*	F11	1.9680	C1-C6	0.0275	27.74	6.63	0.96	0.071
			C5-C6	0.0280	27.74	6.63	0.96	0.071
n -π*	F11	1.9098	C1-C6	0.3671	88.41	21.13	0.42	0.091
n -σ*	N13	1.9226	C3-C12	0.0310	7.24	1.73	0.85	0.035
			C12-H16	0.0408	45.35	10.84	0.82	0.085
			C14-O19	0.0226	39.92	9.54	0.97	0.087
n -π*	N15	1.7363	C14-O19	0.3321	268.78	64.24	0.28	0.121
n -σ*	O19	1.8431	N13-C14	0.0916	114.14	27.28	0.62	0.118
			C14-N15	0.0678	101.34	24.22	0.71	0.12
π*-π*	C1-C6	0.3671	C4-C5	0.2888	922.91	220.58	0.01	0.081

The strong delocalization of lone pair electrons were observed in the interactions of LP N15→π*(C14-O19), LP O19→σ*(N13-C14) and LP O19→σ*(C14-N15) have shown stabilization energies of 268.78, 114.14 and 101.34 KJ/mol, respectively. A moderate stabilization energy of about 88.41 KJ/mol was shown by LP F11→π*(C1-C6) interaction. The orbital overlap between the donors π (C1-C6), (C2-C3), (C4-C5) and acceptors π*(C2-C3), (C4-C5), (C1-C6) orbitals leads to the stabilization energy of ~74 KJ/mol. The intra-molecular interactions were observed an increase in electron density (ED) in (C-C) anti-bonding orbital that weakens the respective bonds. The electron density of conjugated bonds of aromatic ring (1.64e) clearly demonstrates strong delocalization for 4FBU molecule. The bonding orbitals of π(C2-C3) transfer the energy of 83.47 KJ/mol to the anti-bonding orbital of π*(C12-N13). Thus, the π-electron cloud movement from donor to acceptor can make the molecule highly polarized and causes ICT, which is responsible for the NLO activity of 4FBU molecule.

4.4. Energy gap analysis

Frontier molecular orbitals are nothing but the highest occupied molecular orbitals and lowest unoccupied molecular orbitals of the molecule. The LUMO as an electron acceptor represents the ability to obtain an electron; donor represents the ability to donate an electron. The energy gap of HOMO-LUMO explains the eventual charge transfer interaction within the molecule, which influences the biological activity of the molecule. The positive and negative phases are represented in red and green colour

respectively. The energy of the two important FMOs such as the highest occupied molecular orbitals (HOMO), the lowest unoccupied molecular orbitals (LUMO) have been calculated. The frontier molecular orbitals of the title molecule are mapped in Fig (2). The frontier molecular orbitals play an important role in the electric and optical properties, as well as in UV–Vis spectra and chemical reactions. In most cases, even in the absence of inversion symmetry, the strongest bands in the Raman spectrum are weak in the IR spectrum and vice versa. However, the intra-molecular charge transferred from the donor to accepter group through a single–double bond conjugated path can induce large variations of both the molecular dipole moment and the molecular polarizability, making IR and Raman's activity strong at the same time.

As seen from Fig. (2), the HOMO is localized over the Flourine, phenyl and nitrogen atoms within the title molecule, while the LUMO localized all over the title molecule. The analysis of the wave function indicates that the electron absorption corresponds with the transition from the ground to the first excited state and is mainly described by one electron excitation from the HOMO to the LUMO. The energy of HOMO orbital level is 7.2254 eV, and the energy of LUMO orbital level is 2.3371 eV. Hence, the energy gap of the 4FBU molecule is calculated as 4.84835 eV. The lowering of HOMO–LUMO energy gap (4. 84835 eV) reflects the possibility of the intra-molecular charge transfer from HOMO to LUMO. The frontier molecular orbital values are presented in Table 4.

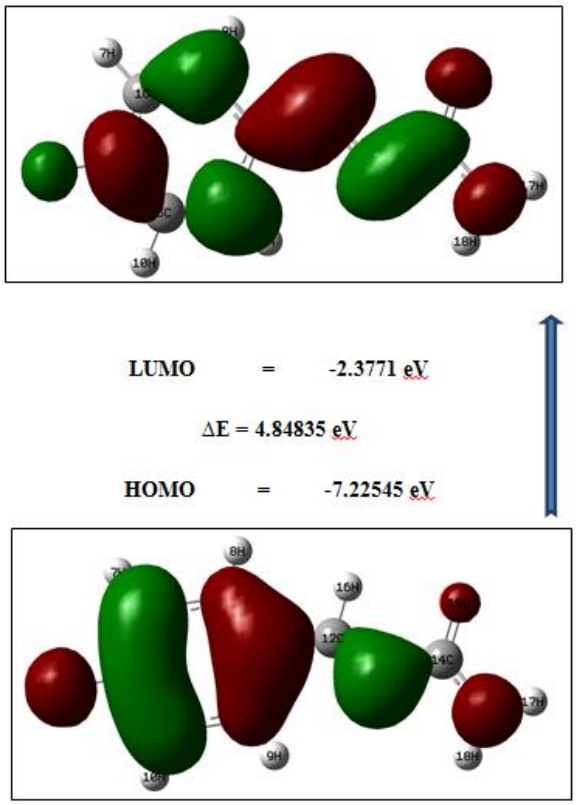

Fig. 2: The Frontier Molecular Orbitals of 4FBU.

Table 4: The Frontier Molecular Orbitals of 4FBU

Orbitals	Energies (a.u)	Energies (eV)
39O	-0.312672	-8.50812
40O	-0.289459	-7.87647
41O	-0.285295	-7.76316
42O	-0.265776	-7.23203
43O	-0.265534	-7.22545
44V	-0.087358	-2.3771
45V	-0.043228	-1.17628
46V	-0.012498	-0.34008
47V	-0.00469	-0.12762
48V	-0.00091	-0.02476

4.5. MEP analysis

MEP and electrostatic potential are useful quantities to illustrate the charge distributions of molecules and used to visualize variably charged regions of a molecule. Therefore, the charge distributions can give information about how the molecules interact with another molecule. The reactive behavior of the 4FBUmolecule is visualized with the help of three-dimensional MEP surface. The molecular electrostatic potential and the electrostatic potential and contour mapped surface of the 4FBU are shown in Fig (3). The total electron density and MEP surface of the molecule under investigation is constructed by using B3LYP/6-31G (d,p) method. MEP surface describes the charge distribution in the molecule and helps in predicting the sites for nucleophilic and electrophilic attack in the molecule. The region of negative charge is pictured out by red colour, which indicates the electrophilic attack sites of our molecule. The red region localized over the carbonyl group of the thio moiety. The region of positive charge is pictured out by blue colour, which indicates the nucleophilic attack sites were localized over two hydrogen atoms of the thiourea side chain. The green colour corresponds to a potential half-way between the two extremes red and blue region and represents the neutral charge. The contour map of 4FBU has shown the electron density rich surface in closed curves, which regions are located over the imine group and the thio moiety present in the title molecule. Which are responsible regions for the activity of the 4FBU molecule.

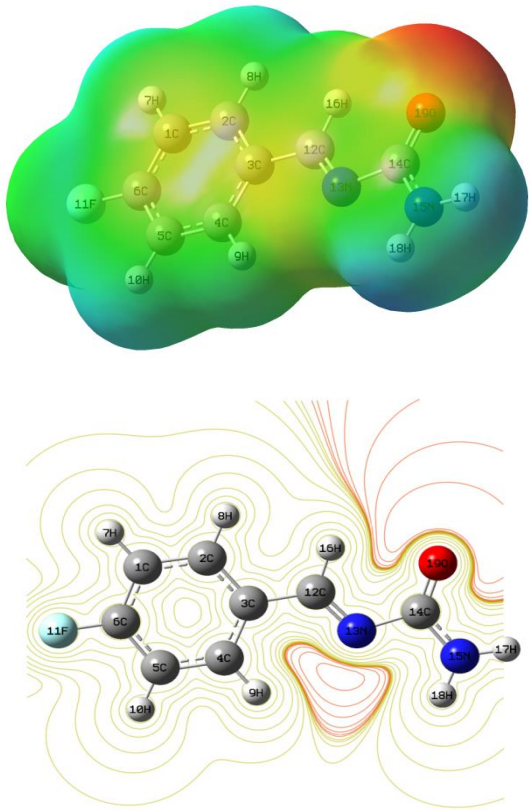

Fig. 3: The Molecular Electrostatic Potential and Contour Mapped Surfaces of 4FBU.

4.6. Vibrational spectral studies

The full description of observed IR and Raman's spectra is presented in Table 5, along with detailed assignment as stipulated by the PED calculation. The observed FT-IR, FT-Raman spectra and the simulated spectra refined by DFT theory are given in Figs. 4 and 5. The theoretical and experimental wavenumbers are in fair agreement and the assignments of wavenumbers for different functional groups are discussed below.

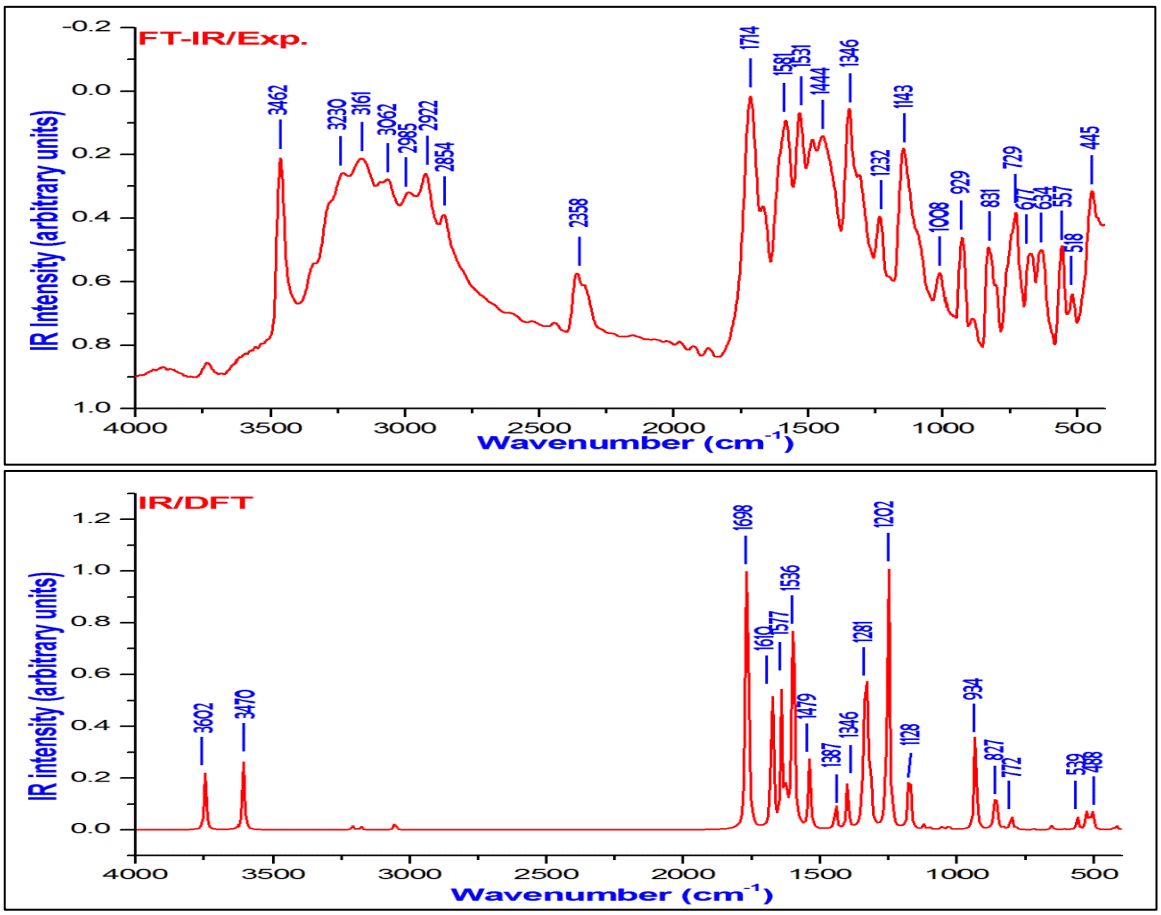

Fig. 4: The Recorded and Simulated FT-IR Spectra of 4FBU.

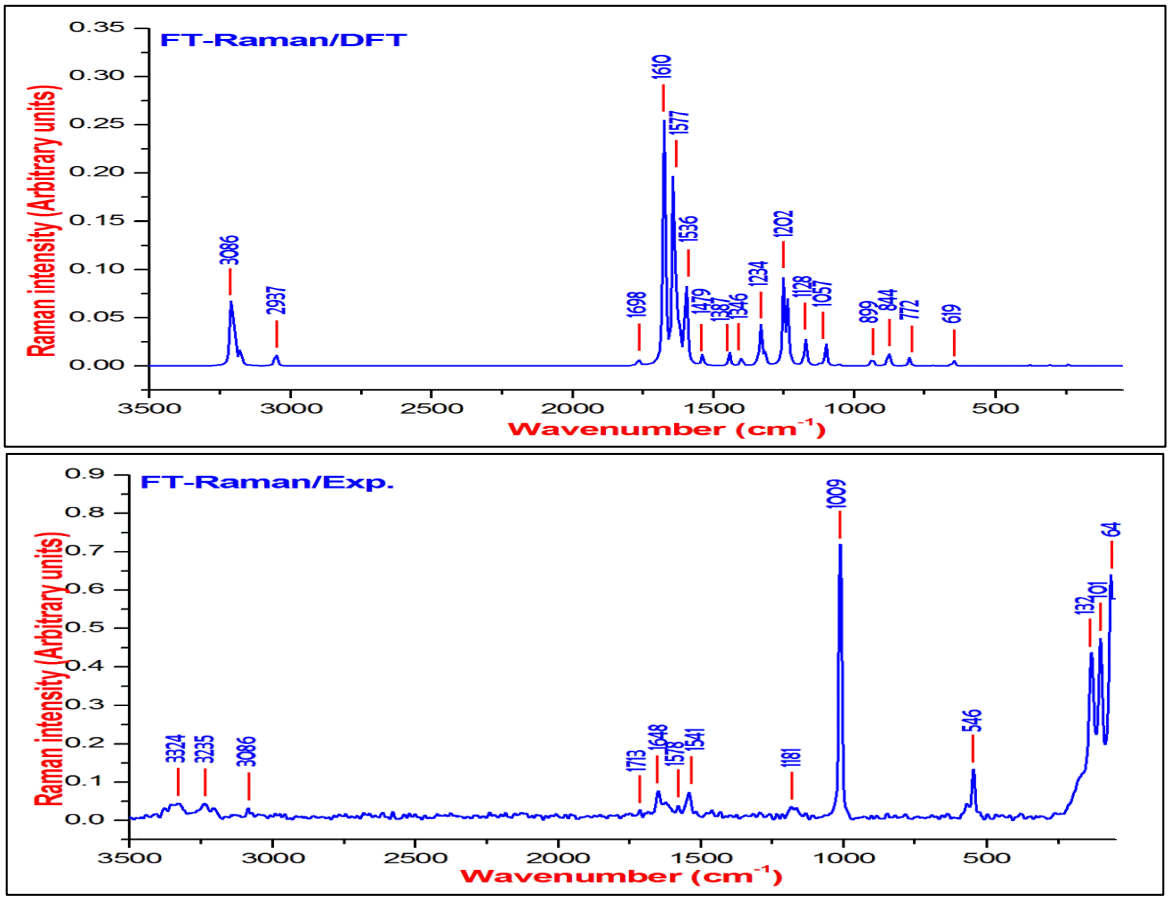

Fig. 5: The Recorded and Simulated FT-Raman Spectra of 4FBU.

Table 5: The Fundamental Vibrational Assignments of 4FBU

Mode No	Theoretical Wavenumber Un Scaled	Scaled	Experimental Wavenumber IR	Raman	IR	Raman	PED≥10%
1	3744	3602			15.2	1.7	$\nu N_{15}H_{17}(100)+\nu N_{15}H_{18}(100)$
2	3607	3470	3462	3324	18.5	5.1	$\nu N_{15}H_{17}(100)+\nu N_{15}H_{18}(100)$
3	3208	3086	3089	3086	0.7	5.8	$\nu C_4H_9(99)+\nu C_5H_{10}(98)$
4	3205	3083			0.4	5.9	$\nu C_1H_7(92)$
5	3195	3074	3062		0.2	2.8	$\nu C_4H_9(99)+\nu C_5H_{10}(98)$
6	3175	3055			0.8	2.2	$\nu C_2H_8(94)$
7	3053	2937	2922		2.3	2.3	$\nu C_{12}H_{16}(100)$
8	1765	1698	1714	1713	100.0	3.0	$\nu O_{19}C_{14}(87)+\nu N_{15}C_{14}(53)$
9	1674	1610	1666	1648	41.3	90.2	$\nu N_{13}C_{12}(62)+\nu C_1C_2(41)+\nu C_4C_5(34)$
10	1639	1577	1581	1578	36.3	100.0	$\nu C_4C_5(68)+\nu C_1C_2(71)+\nu C_2C_3(51)$
11	1622	1560			10.7	19.5	$\nu C_5C_6(67)+\nu C_3C_4(52)+\beta C_2C_1C_6(64)$
12	1596	1536	1531	1541	92.3	41.8	$\beta H_{17}N_{15}H_{18}(82)$
13	1538	1479	1483	1460	21.2	4.4	$\beta C_1C_6C_5(51)+\beta H_7C_1C_2(69)+\beta H_8C_2C_1(79)+\beta H_9C_4C_5(67)+\beta H_{10}C_5C_4(72)$
14	1442	1387			7.8	6.1	$\nu C_4C_5(68)+\nu C_1C_2(71)$
15	1399	1346	1346		12.6	5.5	$\beta H_{16}C_{12}N_{13}(68)$
16	1343	1292	1309	1292	8.1	1.3	$\nu C_5C_6(67)+\nu N_{15}C_{14}(53)$
17	1332	1281			67.4	24.3	$\nu C_5C_6(67)+\nu N_{15}C_{14}(53)+\beta H_{17}N_{15}C_{14}(57)+\beta H_{16}C_{12}N_{13}(68)$
18	1316	1266			22.0	8.0	$\beta H_7C_1C_2(69)+\beta H_8C_2C_1(79)+\beta H_9C_4C_5(67)+\beta H_{10}C_5C_4(72)$
19	1250	1202	1201		78.8	47.6	$\nu C_4C_5(38)+\nu C_1C_2(31)+\nu C_3C_{12}(48)+\nu F_{11}C_6(67)$
20	1235	1188		1181	2.3	36.4	$\nu C_3C_{12}(48)+\nu F_{11}C_6(67)+\beta H_8C_2C_1(79)$
21	1172	1128	1143		24.1	20.2	$\beta H_7C_1C_2(69)+\beta H_8C_2C_1(79)+\beta H_9C_4C_5(67)+\beta H_{10}C_5C_4(72)$
22	1119	1077			1.4	1.8	$\nu C_4C_5(68)+\nu C_1C_2(71)+\beta H_7C_1C_2(69)+\beta H_8C_2C_1(79)+\beta H_9C_4C_5(67)$
23	1099	1057			0.9	14.5	$\nu O_{19}C_{14}(87)+\beta H_{17}N_{15}C_{14}(57)$
24	1053	1013			1.3	1.7	$\Gamma H_{16}C_{12}N_{13}C_{14}(84)$
25	1028	989	1008	1009	1.4	0.2	$\beta C_1C_6C_5(51)+\beta C_2C_1C_6(64)+\beta C_4C_5C_6(65)$
26	990	953			0.0	0.0	$\Gamma H_7C_1C_2H_8(84)+\tau C_4C_3C_5H_9(75)+\Gamma H_{10}C_5C_6F_{11}(83)$
27	961	925	929		0.0	0.0	$\Gamma H_7C_1C_2H_8(84)$
28	934	899	891		29.4	8.3	$\nu N_{13}C_{14}(51)+\beta C_3C_{12}N_{13}(76)$
29	877	844	831		0.5	16.2	$\nu C_2C_3(51)+\nu C_3C_4(52)+\nu C_5C_6(67)$
30	860	827			15.5	0.1	$\Gamma H_7C_1C_6F_{11}(82)+\tau C_4C_3C_5H_9(75)+\Gamma H_{10}C_5C_6F_{11}(83)+\Gamma C_1C_6C_4C_5(77)$
31	831	799	804		0.5	0.0	$\Gamma H_7C_1C_6F_{11}(82)+\tau C_4C_3C_5H_9(75)+\Gamma H_{10}C_5C_6F_{11}(83)$
32	803	772			4.7	8.4	$\nu F_{11}C_6(67)+\beta C_2C_3C_4(64)$
33	782	753			0.6	0.2	$\Gamma C_3C_{12}N_{13}C_{14}(80)+\tau O_{19}N_{13}N_{15}C_{14}(82)$
34	718	691	677		0.4	0.9	$\Gamma C_1C_6C_2C_3(89)+\Gamma C_1C_6C_4C_5(77)+\tau O_{19}N_{13}N_{15}C_{14}(82)+\tau F_{11}C_1C_5C_6(88)$
35	655	631	634		1.1	1.7	$\beta N_{13}C_{14}O_{19}(65)+\beta C_4C_5C_6(65)$
36	644	619			0.3	7.7	$\beta C_1C_6C_5(51)+\beta N_{13}C_{14}O_{19}(65)+\beta C_4C_5C_6(65)$
37	608	585			0.3	0.1	$\Gamma H_{17}N_{15}C_{14}N_{13}(92)$
38	561	539		546	3.3	0.8	$\beta C_3C_{12}N_{13}(76)+\beta N_{13}C_{14}N_{15}(73)+\beta C_2C_3C_{12}(65)$
39	525	505	518		6.8	0.3	$\Gamma C_3C_2C_4C_5(83)+\tau F_{11}C_1C_5C_6(88)$
40	507	488			7.2	0.6	$\beta C_1C_6C_5(51)+\beta N_{13}C_{14}N_{15}(73)$
41	429	413			0.4	0.2	$\Gamma C_1C_6C_2C_3(89)+\Gamma C_3C_2C_4C_5(83)$
42	417	401			1.0	0.2	$\beta C_2C_1C_6(64)+\beta C_5C_6F_{11}(67)$
43	377	363			2.2	3.2	$\Gamma C_1C_6C_4C_5(77)+\tau F_{11}C_1C_5C_6(88)+\Gamma C_5C_4C_3C_{12}(87)$
44	309	297			2.2	4.8	$\beta N_{13}C_{14}N_{15}(73)+\beta C_2C_3C_{12}(65)$
45	243	234			52.5	0.8	$\tau N_{15}H_{17}C_{14}H_{18}(89)$
46	240	231			0.7	6.8	$\nu C3C12(48)+\beta N_{13}C_{14}O_{19}(65)+\beta C_2C_3C_4(64)+\beta C_{12}N_{13}C_{14}(62)$
47	202	194			0.5	2.0	$\Gamma C_4C_3C_{12}N_{13}(79)+\Gamma C_1C_6C_4C_5(77)+\Gamma C_3C_2C_4C_5(83)+\Gamma C_3C_{12}N_{13}C_{14}(80)$
48	152	146		132	1.3	0.6	$\Gamma C_4C_3C_{12}N_{13}(79)+\Gamma C_{12}N_{13}C_{14}N_{15}(96)+\Gamma C_3C_{12}N_{13}C_{14}(80)$
49	95	91		101	0.3	3.0	$\beta C_3C_{12}N_{13}(76)+\beta C_2C_3C_{12}(65)+\beta C_{12}N_{13}C_{14}(62)$
50	64	62			0.2	1.2	$\Gamma C_1C_6C_4C_5(77)+\Gamma C_3C_{12}N_{13}C_{14}(80)+\Gamma C_5C_4C_3C_{12}(87)$
51	32	31			2.2	3.0	$\Gamma C_4C_3C_{12}N_{13}(79)+\Gamma C_{12}N_{13}C_{14}N_{15}(96)$

4.6.1. C=O Vibrations

The C=O stretching vibration band can be easily identified from the IR and Raman spectrum. Because of the degree of conjugation, the strength and polarizations are also increasing. The carbonyl vibrations bands in ketones normally show strong intensity and are expected in the region 1715–1680 cm^{-1} (Smith, 1998). The strong band observed at 1714 cm^{-1} in FT-IR and a weak band observed at 1713 cm^{-1} in FT-Raman spectrum are assigned to the carbonyl stretching vibration of the 4FBU molecule. The theoretical wavenumber at 1698 cm^{-1} corresponds to the same vibration with 87% of PED contribution along with νCN stretching vibration. The both observed and calculated values are coincides well with each other. The intensity of the carbonyl group can increase by the conjugation or formation of hydrogen bonds.

4.6.2. C=N and C-N Vibrations

The identification of C=N and C−N stretching in the side chain is a rather difficult task since there are problems in identifying these frequencies from other vibrations. Clougherty et al. 1957, have assigned the C=N stretching frequency in benzylidene anilines to the region 1610-1630 cm^{-1}. In our present study, the C=N stretching vibration observed as a weak band at 1666 cm^{-1} in FT-IR and at 1648 cm^{-1} in FT-Raman spectrum. The wavenumber calculated at 1610 cm^{-1} shown deviation with experimental wavenumber due to the mixing of νCC vibrations of the phenyl ring. Silverstein et al. 1981 assigned C–N stretching vibrations in the region 1382–1266 cm^{-1} for the aromatic amines. Herein, the C-N stretching vibrations are identified as weak bands in both FT-IR (1309 cm^{-1}) and FT-Raman (1292 cm^{-1}) spectrum. The calculated wavenumber at 1292 cm^{-1} shows very good agreement with each other. The vibration observed at 1346 cm^{-1} in FT-IR spectrum and its corresponding harmonic wavenumber computed at 1346 cm^{-1} are assigned to βCNH bending vibration.

4.6.3. N-H Vibrations

The N−H stretching vibration appears strongly and broadly in the region 3500–3300 cm^{-1} (Erdoğdu et al. 2008). In this study, the amino group stretching vibration is observed at very strong band at 3462 cm^{-1} in FT-IR spectrum and as weak band at 3324 cm^{-1} in

FT-Raman spectrum, respectively. The wavenumber calculated at 3470 cm^{-1} assigned to the N-H vibration of the title molecule. The PED corresponding to this vibration is a pure mode and is exactly contributes about to 100%. The symmetric deformation of NH_2 usually occurs as a strong band in the region 1580–1650 cm^{-1}. The strong deformation observed at 1531 and 1541 cm^{-1} in FT-IR and FT-Raman spectrum is assigned to NH_2 deformation vibration of the title molecule and its corresponding theoretical wavenumber shows good covenant with 1536 cm^{-1}.

4.6.4. C−F Vibrations

The C−F group gives rise to its stretching wavenumber in the region 1000–1450 cm^{-1} and usually appears with strong intensity in both Raman and infrared spectra (Páez Jerez et al. 2015). For the title compound the band observed at 1201 cm^{-1} is assigned for the C-F stretching vibration and this vibration mixed with the C-C vibrations of the phenyl ring with considerable PED contribution ~38%. The wavenumber computed at 1202 cm^{-1} is corresponds to the C-F stretching vibration of the title molecule. The C–F in-plane bending wavenumber appears in the region 700–850 cm^{-1}. The FT-IR bands at 831 and 804 cm^{-1} are corresponds to the in-plane bending vibrations of the fluorine atom. The theoretical wavenumber at 827 and 799 agree well with the experimental findings. The C-F out-of-plane bending vibrations are computed at 505 cm^{-1} and the band observed at 501 cm^{-1} in FT-IR spectrum are assigned appropriately.

4.6.5. Ring Vibrations

The aromatic CH-stretching vibrations absorb weakly to moderately between 3120 and 3000 cm^{-1} (Roeges, 1994). The DFT calculations gives the bands at 3086-3055 cm^{-1} are assigned to the C-H stretching vibrations of the phenyl ring. The experimental wavenumbers observed 3089, 3062 cm^{-1} in FT-IR and at 3086 cm^{-1} in FT-Raman spectrum are corresponds to the C-H vibrations. In this region, the TED calculations show that all the C–H stretching vibrations are pure modes. The C-H vibration of azomethine group is observed as strong band at 2922 cm^{-1} in FT-IR spectrum and its theoretical wavenumber computed at 2937 cm^{-1} shows good agreement with each other. The carbon–carbon stretching modes of the phenyl group are expected in the range of 1620 to 1320 cm^{-1} (Faniran&Shurvell, 1968). In the present study, the carbon–carbon stretching vibrations of the 4FBU have been observed at 1581, 1483, 1309 cm^{-1} in FT-IR and at 1578, 1460, 1292 cm^{-1} in FT-Raman are corresponding bands for the C−C vibrations of the aromatic ring. The wavenumbers at 1577, 1560, 1479 and 1292 cm^{-1} from the B3LYP calculations are assigned to the ring C-C vibrations of the title molecule. The ring-breathing mode for the para substituted benzenes with entirely different substituents has been reported to be strongly IR active with typical bands in the interval 780–840 cm^{-1} (Varsanyi, 1974). The ring breathing mode and trigonal bending vibration of the phenyl were observed at 1008, 831cm^{-1} in FT-IR and 1009 cm^{-1} in FT-Raman spectrum. The theoretical wavenumber corresponds to these vibrations obtained at 989 and 844 cm^{-1}.

4.7. Light harvesting efficiency calculations

The excitation energies, absorbance and oscillator strengths for the title molecule at the optimized geometry were computed and tabulated in Table 6. The highest band observed at 305 nm with an oscillator strength of f=0.5055 corresponds to the transition of HOMO-1 to LUMO. From the three excitations predicted by TD-DFT, two have non-negligible oscillator strengths f>0.1. The oscillator strength G reflects the strength of the particular transition; in other words, the light harvesting efficiency (LHE). The values of f determine the usefulness of sensitizer in DSSC (Wang et al. 2013; Heera&Cindrella, 2009). Relationship of LHE to f is expressed as:

$$LHE = 1-10^{-f} \quad (8)$$

Table 6: The Oscillator Strength, Excitation Energies and Transitions of 4FBU

Excited States	CI expansion coefficient	Energy gap	Gas phase	Oscillator strength
Excited State1:				
43→44	0.6967	3.6503 eV	339.66 nm	f=0.0003
Excited State2:				
40→44	0.1141			
42→44	0.6842	4.7268 eV	262.30 nm	f=0.5055
Excited State3:				
40→44	0.6029	4.7859 eV	259.06 nm	f=0.0267
42→44	-0.1101			
42→45	-0.3471			

The light harvesting efficiency of 4FBU is calculated as 0.6877, which shows the capability to capture photons and exhibiting the photon-energy conversion efficiency. The light harvesting efficiency 0.6877 reveals that 4FBU have sensitizing application in dye sensitized solar cells. The theoretical absorption maximum peak of the 4FBU is shown in Fig. 6.

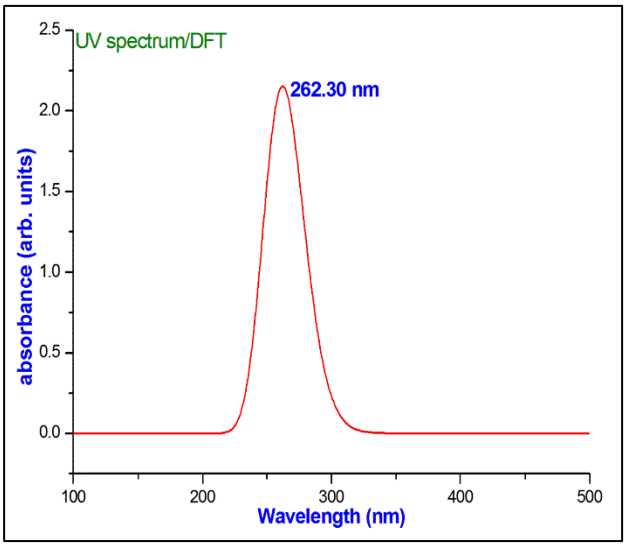

Fig. 6: The Absorption Maximum Peak of 4FBU Calculated by DFT Method.

4.8. Mulliken atomic charges

Mulliken atomic charge calculation has an important role in the application of quantum chemical calculation to molecular system, since atomic charges affect the dipole moment, molecular polarizability, electronic structure and more a lot of properties of molecular systems. The Mulliken charges were calculated by DFT/B3LYP/6-31G(d,p) basis set. The calculated Mulliken charge values are listed in Table 7 and are plotted in Fig. 7. In our study, the carbon atoms have most positive (C3: 0.74847) and most negative charge (C2: -1.09447). The lone pair atoms such as N, O and F have negative charges. All the hydrogen atoms have positive charge.

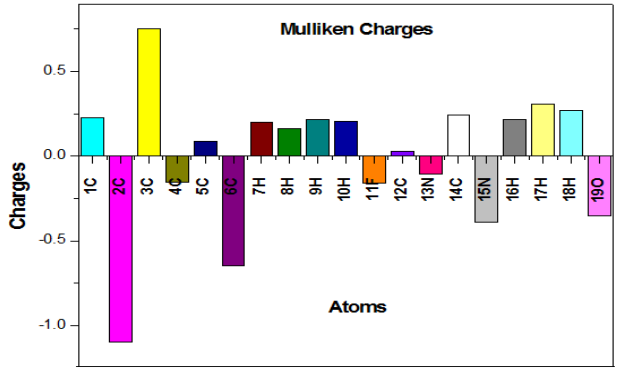

Atoms	Charges	Atoms	Charges
1C	0.224137	11F	-0.15987
2C	-1.09447	12C	0.027733
3C	0.74847	13N	-0.105321
4C	-0.154701	14C	0.240205
5C	0.086297	15N	-0.389476
6C	-0.647069	16H	0.217425
7H	0.201226	17H	0.30784
8H	0.161171	18H	0.266044
9H	0.214749	19O	-0.349516
10H	0.205125		

Table 7: The Mulliken Atomic Charges of 4FBU
Fig. 7: The Mulliken Atomic Charges Plot of 4FBU.

4.9. Thermodynamic properties

On the basis of vibrational analysis, the statistical thermodynamic functions heat capacity ($C^0_{p,\ m}$), entropy (S^0_m), and enthalpy changes (ΔH^0_m) for the 4FBU were obtained from the theoretical harmonic frequencies listed in Table 8. It can be seen from Table 8, the thermodynamic functions are increasing with temperature ranging from 100 to 1000 K due to the fact that the molecular vibrational intensities increase with temperature. The correlation equations between heat capacity, entropy, enthalpy changes and temperatures were fitted by quadratic formulas and the corresponding fitting factors (R^2) for these thermodynamic properties are 0.99895, 0.99997 and 0.99946, respectively. The comparative thermodynamical graphs of 4FBU are shown in Fig. 8. The corresponding fitting equations are as follows:

$$C^0_{p,m} = 5.42703 + 0.02291T + 2.0243x10^{-5}\ T^2\ (R^2 = 0.99895)$$

$$S^0_m = 1.24898 + 0.00527T + 4.65873x10^{-5}\ T^2\ (R^2 = 0.99997)$$

$$\Delta H^0_m = 3.05729 + 0.01291T + 1.14038x10^{-5}\ T^2\ (R^2 = 0.99946)$$

All the given thermodynamic data are the helpful information for further study on 4FBU. If can be used to compute the other thermodynamic energies according to relationships of thermodynamic functions and estimate directions of chemical reactions according to the second law of thermodynamics in thermochemical field. All the thermodynamic calculations were done in gas phase and they could not be used in solution.

Table 8: Thermodynamic Properties of 4FBU at Different Temperatures

T (K)	S (J/mol.K)	Cp (J/mol.K)	ΔH (KJ/mol)
100	341.24	97.36	6.77
200	425.36	153.35	19.22
298.15	498.26	216.68	37.35
300	499.6	217.89	37.75
400	570.98	279.98	62.71
500	639.27	332.23	93.41
600	703.68	374.06	128.81
700	763.94	407.38	167.94
800	820.16	434.28	210.07
900	872.62	456.34	254.64
1000	921.68	474.68	301.21

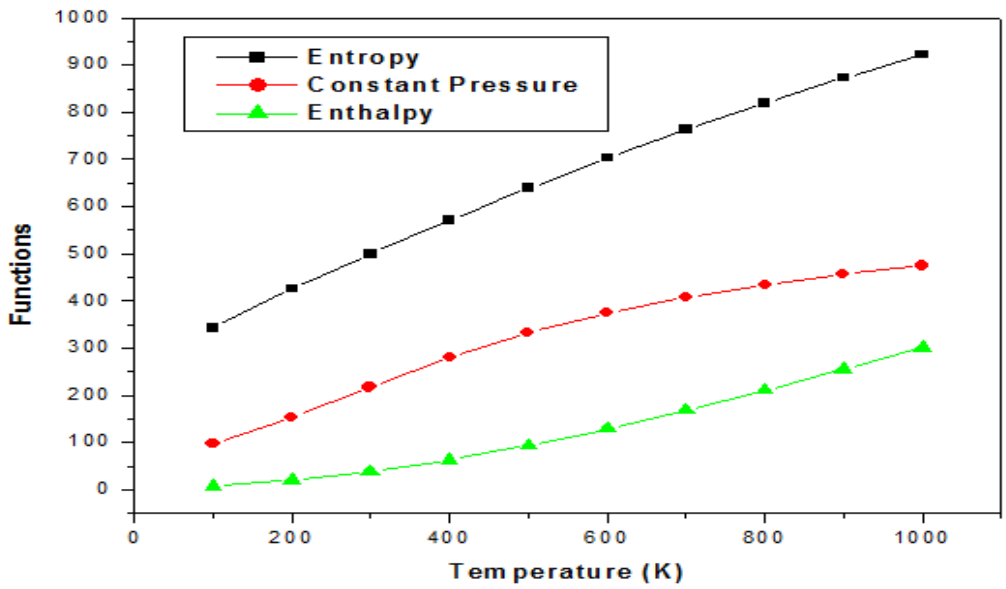

Fig. 8: The Thermodynamic Properties of 4FBU at Different Temperatures.

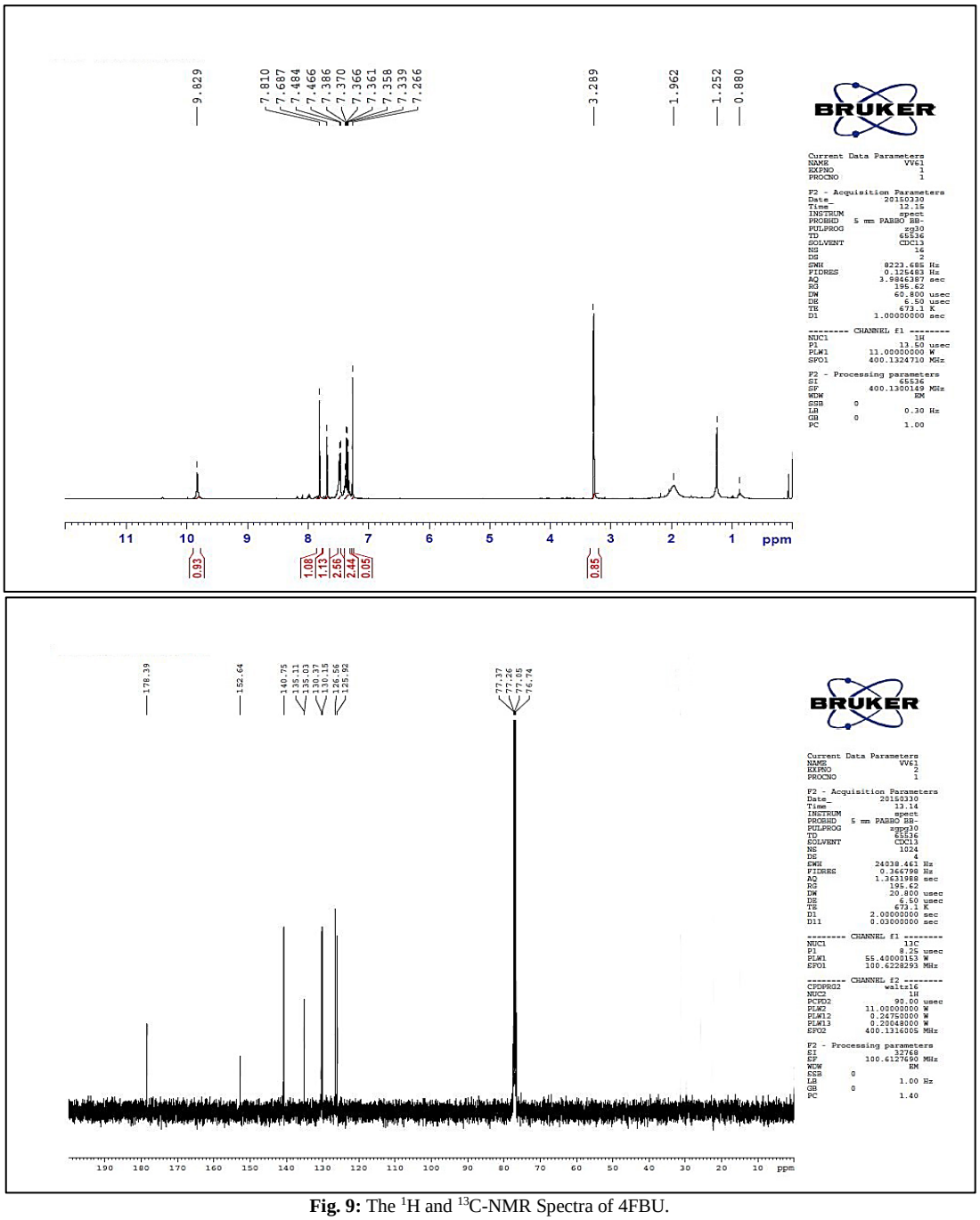

Fig. 9: The ^{1}H and ^{13}C-NMR Spectra of 4FBU.

5. Conclusion

A complete vibrational analysis was carried out for the first time to the molecule 4FBU. The optimized bond parameters were calculated at DFT/B3LYP/6-31G (d,p) method. The observed FT-IR and FT-Raman spectral values were in good agreement with the calculated values. The first order hyperpolarizability (β_0=10.5890x10^{-30}esu) of 4FBU was calculated and found to be twentyeight times greater than that of urea and hence the molecule possesses considerable NLO activity. NBO study reveals that theπ-electron cloud movement from donor to acceptor can make the molecule highly polarized and causes ICT, which is responsible for the NLO activity of 4FBU molecule. The light harvesting efficiency 0.6877 reveals that 4FBU have sensitizing application in dye sensitized solar cells. MEP surface analysis mentioned the active charge sites of the molecule 4FBU. In addition, Mulliken charges and thermodynamic properties were also reported.

References

[1] Charles, D. Lowry, Jr., U.S. 2,715,073, 1955.

[2] CompagnicFranosisedereaffinage, Fr. 1,122,357, 1956.

[3] Mounika,K., Pragathi, A., Gyanakumar,C.,2010, Synthesis, Characterization and Biological Activity of a Schiff Base Derived from 3-Ethoxy Salicylaldehyde and 2-Amino Benzoic acid and its Transition Metal Complexes, J. Sci. Res. 2 (3), 513-524, https://doi.org/10.3329/jsr.v2i3.4899.

[4] Venkatesh, P., 2011, Synthesis, characterization and antimicrobial activity of various schiff bases complexes of Zn (II) and Cu (II) ions. Asian J Pharm Hea Sci. 1(1):8–11.

[5] Yıldız, M., Dülger, B., Koyuncu, S.Y., Yapici, B.M., 2004, Synthesis and antimicrobial activity of bis (imido) Schiff bases derived from thiosemicarbazide with some 2-hydroxyaldehydes and metal complexes, J. Ind. Chem. Soc., 81 7-12.

[6] Ünver, H., Yıldız, M., Dülger, B., Özgen, Ö., Kendi, E., & Durlu, T.N., 2005, Spectroscopic studies, antimicrobial activities and crystal structures of N-(2-hydroxy-3-methoxybenzalidene)1-

aminonaphthalene. Journal of Molecular Structure, 737(2-3), 159–164. https://doi.org/10.1016/j.molstruc.2004.10.030.

[7] Yıldız, M., Ünver, H., Dülger, B., Erdener, D., Ocak, N., Erdönmez, A., &Durlu, T. N., 2005, Spectroscopic study, anti-microbial activity and crystal structures of N-(2-hydroxy-5-nitro benzalidene)4-aminomorpholine and N-(2-hydroxy-1-naphthylidene)4-aminomorpholine. Journal of Molecular Structure, 738(1-3), 253–260. https://doi.org/10.1016/j.molstruc.2004.10.029.

[8] Yıldız, M.,Dülger, B., Çınar, A., 2005, Synthesis and characterization of new crown ethers of Schiff base type and their complexes, J. Ind. Chem. Soc. 82, 414-420.

[9] Yildiz, M., Kİraz, A., &Dülger, B. (2007). Synthesis and anti-microbial activity of new crown ethers of Schiff base type. Journal of the Serbian Chemical Society, 72(3), 215–224. https://doi.org/10.2298/JSC0703215Y.

[10] Kiraz, A., Yıldız, M., Dülger, B., 2009, Synthesis and Characterization of Crown Ethers, Asian J. Chem. 21, 6, 4495-4507.

[11] Sondhi, S.M., Singh, N., Kumar, A., Lozach, O., Meijer, L., 2006, Synthesis, anti-inflammatory, analgesic and kinase (CDK-1,CDK-5 &GSK-3) inhibition activity evaluation of benzimidazole /benzoxazole derivatives and some Schiff's bases, Bio-organic & MedicinalChemistry, 14(11), 3758–3765, https://doi.org/10.1016/j.bmc.2006.01.054.

[12] Cozzi, P.G., 2004, Metal–Salen Schiff base complexes in catalysis: practical aspects. Chem. Soc. Rev., 33(7), 410–421. https://doi.org/10.1039/B307853C.

[13] Chandra, S., Sangeetika, J., 2004, EPR and electronic spectral studies on copper (II) complexes of some NO donor ligands, J. Indian Chem. Soc. 81, 203-206.

[14] Whitnall, M., & Richardson, D.R., 2006, Iron: A New Target for Pharmacological Intervention in Neurodegenerative Diseases. Seminars in Pediatric Neurology, 13(3), 186–197. https://doi.org/10.1016/j.spen.2006.08.008.

[15] Spek, A.L., 1998, PLATON, A Multipurpose Crystallographic Tool, Utrecht University, Utrecht, the Netherlands.

[16] Pérez-Rebolledo, A., Piro, O.E., Castellano, E.E., Teixeira, L.R., Batista, A. A., &Beraldo, H., 2006, Metal complexes of 2-benzoylpyridine semicarbazone: Spectral, electrochemical and structural studies. Journal of Molecular Structure, 794(1-3), 18–23. https://doi.org/10.1016/j.molstruc.2006.01.032.

[17] Buss, J.L., Neuzil, J., &Ponka, P., 2002, the role of oxidative stress in the toxicity of pyridoxal isonicotinoylhydrazone (PIH) analogues. Biochemical Society Transactions, 30(4), 755–758. https://doi.org/10.1042/bst0300755.

[18] Kaya, I., &Kamaci, M., 2012, Synthesis, optical, electrochemical, and thermal stability properties of poly (azomethine-urethane)s. Progress in Organic Coatings, 74(1), 204–214. https://doi.org/10.1016/j.porgcoat.2011.12.010.

[19] Dinçalp, H., Yavuz, S., Haklı, Ö, Zafer, C., Özsoy, C., Durucasu, İ., &İçli, S., 2010, Optical and photovoltaic properties of salicylaldimine-based azo ligands. Journal of Photochemistry and Photobiology A: Chemistry, 210(1), 8–16. https://doi.org/10.1016/j.jphotochem.2009.12.012.

[20] Frisch, M.J., Trucks, G.W., Schlegel, H.B., Scuseria, G.E., Robb, M.A., 2004, Theoretical and Computational Aspects of Magnetic Organic Molecules. Gaussian Inc, Wallingford, CT.

[21] Schlegel, H.B., 1982, Optimization of equilibrium geometries and transition structures. Journal of Computational Chemistry, 3(2), 214–218. https://doi.org/10.1002/jcc.540030212.

[22] Jamróz, M.H., Dobrowolski, J.C., &Brzozowski, R., 2006, Vibrational modes of 2, 6-, 2, 7-, and 2, 3-diisopropylnaphthalene. A DFT study. Journal of Molecular Structure, 787(1-3), 172–183. https://doi.org/10.1016/j.molstruc.2005.10.044.

[23] Michalska, D., 2003, Raint Program, Wroclaw University of Technology, Poland.

[24] Michalska, D., &Wysokiński, R., 2005, the prediction of Raman spectra of platinum (II) anticancer drugs by density functional theory. Chemical Physics Letters, 403(1-3), 211–217. https://doi.org/10.1016/j.cplett.2004.12.096.

[25] Kleinman, D.A., 1962, Nonlinear Dielectric Polarization in Optical Media. Physical Review, 126(6), 1977–1979. https://doi.org/10.1103/PhysRev.126.1977.

[26] Alyar, H., Kantarci, Z., Bahat, M., &Kasap, E., 2007, Investigation of torsional barriers and nonlinear optical (NLO) properties of phenyltriazines. Journal of Molecular Structure, 834-836, 516–520. https://doi.org/10.1016/j.molstruc.2006.11.066.

[27] Castiglioni, C., Del Zoppo, M., Zuliani, P., &Zerbi, G., 1995, Experimental molecular hyperpolarizabilities from vibrational spectra in systems with large electron-phonon coupling. Synthetic Metals, 74(2), 171–177. https://doi.org/10.1016/0379-6779(95)03364-5.

[28] Zuliani, P., Del Zoppo, M., Castiglioni, C., Zerbi, G., Marder, S.R., & Perry, J.W., 1995, Solvent effects on first-order molecular hyperpolarizability: A study based on vibrational observables. The Journal of Chemical Physics, 103(23), 9935–9940. https://doi.org/10.1063/1.469882.

[29] Del Zoppo, M., Castiglioni, C., &Zerbi, G., 1995, Response to the "comment on 'non-linear optical response to strong applied electromagnetic fields in polyconjugated materials' by M. Del Zoppo, C. Castiglioni, G. Zerbi, M. Rui and M. Gussoni" by D.M. Bishop. Synthetic Metals, 68(3), 295–296. https://doi.org/10.1016/0379-6779(94)02327-U.

[30] Del Zoppo, M., Castiglioni, C., Zuliani, P., Razelli, A., Zerbi, G., Blanchard-Desce,M., 1998, Use of vibrational spectra for the determination of first-order molecular hyperpolarizabilities of push–pull polyenes as function of structural parameters, *J. Appl. Polym. Sci.*, 70, 1311–1320. https://doi.org/10.1002/(SICI)1097-4628(19981114)70:7<1311::AID-APP8>3.0.CO;2-P.

[31] Ravikumar, C., Joe, I.H., & Jayakumar, V.S., 2008, Charge transfer interactions and nonlinear optical properties of push–pull chromophore benzaldehyde phenylhydrazone: A vibrational approach. Chemical Physics Letters, 460(4-6), 552–558. https://doi.org/10.1016/j.cplett.2008.06.047.

[32] Reed, A.E., &Weinhold, F., 1985, Natural localized molecular orbitals. The Journal of Chemical Physics, 83(4), 1736–1740. https://doi.org/10.1063/1.449360.

[33] Reed, A.E., Weinstock, R.B., &Weinhold, F., 1985, Natural population analysis. The Journal of Chemical Physics, 83(2), 735–746. https://doi.org/10.1063/1.449486.

[34] Reed, A.E., &Weinhold, F., 1983, Natural bond orbital analysis of near-Hartree–Fock water dimer. The Journal of Chemical Physics, 78(6), 4066–4073. https://doi.org/10.1063/1.445134.

[35] Foster, J.P., &Weinhold, F., 1980, Natural hybrid orbitals. Journal of the American Chemical Society, 102(24), 7211–7218. https://doi.org/10.1021/ja00544a007.

[36] Chocholoušová, J., Špirko, V., &Hobza, P., 2004, First local minimum of the formic acid dimer exhibits simultaneously red-shifted O–H···O and improper blue-shifted C–H···O hydrogen bonds. Phys. Chem. Chem. Phys., 6(1), 37–41. https://doi.org/10.1039/B314148A.

[37] Smith, B., 1998, Infrared Spectral Interpretation: A Systematic Approach, CRC Press, Washington, DC.

[38] Clougherty, L., Sousa, J., & Wyman, G., 1957, Notes - C=N Stretching Frequency in Infrared Spectra of Aromatic Azomethines. The Journal of Organic Chemistry, 22(4), 462–462. https://doi.org/10.1021/jo01355a618.

[39] Silverstein, M., Clayton Basseler, G., Morill, C., 1981, Spectrometric Identification of Organic Compounds, Wiley, New York.

[40] Erdoğdu, Y., Güllüoğlu, M.T., &Yurdakul, S., 2008, Molecular structure and vibrational spectra of 1, 3-bis (4-piperidyl) propane by quantum chemical calculations. Journal of Molecular Struct, 889(1-3), 361–370. https://doi.org/10.1016/j.molstruc.2008.02.019.

[41] Páez Jerez, A.L., Flores Antognini, A., Cutin, E.H., & Robles, N.L., 2015, Synthesis, characterization and vibrational properties of p-fluorosulfinylaniline. Spectrochimica Acta Part A: Molecular and Biomolecular Spectroscopy, 137, 300–305. https://doi.org/10.1016/j.saa.2014.08.040.

[42] Roeges, N.P.G., 1994, A Guide to the Complete Interpretation of Infrared Spectra of Organic Structures. Wiley: New York.

[43] Faniran, J.A., &Shurvell, H.F., 1968, Infrared spectra of phenylboronic acid (normal and deuterated) and diphenyl phenylboronate. Canadian Journal of Chemistry, 46(12), 2089–2095. https://doi.org/10.1139/v68-341.

[44] Varsanyi, G., 1974, Assignments of Vibrational Spectra of Seven Hundred Benzene Derivatives.Wiley: New York.

[45] Wang, J., Cong, S., Wen, S., Yan, L., & Su, Z., 2013, A Rational Design for Dye Sensitizer: Density Functional Theory Study on the Electronic Absorption Spectra of Organoimido-Substituted Hexamolybdates. The Journal of Physical Chemistry C, 117(5), 2245–2251. https://doi.org/10.1021/jp3106452.

[46] Heera, T.R., & Cindrella, L., 2009, Molecular orbital evaluation of charge flow dynamics in natural pigments based photosensitizers. Journal of Molecular Modeling, 16(3), 523–533. https://doi.org/10.1007/s00894-009-0569-z.